Alnasif *et al. Carbon Neutrality* (2022) 1:24
https://doi.org/10.1007/s43979-022-00021-9

Carbon Neutrality

ORIGINAL ARTICLE

Open Access

Experimental and numerical analyses of nitrogen oxides formation in a high ammonia-low hydrogen blend using a tangential swirl burner

A. Alnasif[1,2*], S. Mashruk[1], M. Kovaleva[1], P. Wang[3] and A. Valera-Medina[1]

Abstract

Ammonia has been considered as a novel fuel for decarbonization purposes. However, emissions from combustion systems are still posing a problem. Therefore, experimental and numerical simulations have been conducted to study the concentration of exhaust emissions (Nitric oxide "NO", Nitrous oxide "N_2O") from burning the ammonia/hydrogen (NH_3/H_2) blend 85/15 (vol%). The effects were measured at various thermal powers ranging 10 to 20 kW and with different Reynolds numbers from 20,000—40,000. The experimental points were numerically investigated in the Ansys CHEMKIN-Pro environment employing seven chemical kinetic mechanisms taken from the literature. All experiments have been undertaken at standard atmospheric conditions. The experimental results showed that both NO and N_2O gradually increased when the Reynolds number increased from 20,000 to 40,000. Along with that, the concentration of NO emissions at the exhaust reported minimum level when the Re = 20,000 due to lower reactivity radical formation, all that led to a deterioration of the flame characteristics. Also, the integrated radical intensities of NO*, OH*, NH*, and NH_2* demonstrate an increasing trend as Re increased from 20,000 to 40,000. In terms of thermal power, N_2O suffered an abrupt decrease when the thermal power increased up to 15 kW, while the opposite occurs for NO. In addition, the radicals intensity of OH*, NH*and NH_2* figures show an increase in their concentration when the thermal power increased up to 15 kW then decreased with increasing thermal intensity to reach 20 kW, reflecting into increased NO productions and decreased N_2O levels. The numerical analysis showed that Stagni, Bertolino, and Bowen Mei were the most accurate mechanisms as these give a good prediction for NO and N_2O. The study also showed that the chemical reaction ($HNO + O_2 \leftrightarrow NO + HO_2$) is the main source of NO formation. While the chemical reaction ($NH + NO \leftrightarrow N_2O + H$) is responsible for the formation of N_2O by consuming NO and when there will be abundance in NH radicals. Finally, dealing with a blended fuel of high ammonia concentration encourages ammonia chemistry to become more dominant in the flame. It decreases the flame temperature, hence lowering heat loss between the flame and the surrounding.

Keywords: Ammonia, N_2O, NO, Chemiluminescence, Kinetic modeling

1 Introduction

Reducing carbon dioxide (CO_2) emissions is the primary goal towards the transition to an environmentally friendly future that does not depend on fossil fuels. Out of the potential sources that can replace fossils, ammonia is one of the most attractive candidates that has drawn considerable attention, leading to many studies that

*Correspondence: alnasifah@cardiff.ac.uk

[1] College of Physical Sciences and Engineering, Queen's Building, Cardiff University, Cardiff, Wales CF243AA, UK
Full list of author information is available at the end of the article

analyze the molecule as a promising free-carbon energy carrier [1, 2]. The role of ammonia as a carbon-free fuel and its potential as a source to leverage excess energy from renewable energy has encouraged numerous studies in engines and gas turbines [3, 4]. These studies have complemented essential combustion analyses to determine flame propagation and ignition delay time in pure and blended ammonia mixtures.

The combustion characteristics of ammonia (NH_3) when it is injected directly as pure ammonia into the combustion system differs from standard hydrocarbon fuels: the higher ignition delay time, higher heat of vaporization, higher minimum ignition energy, low burning velocity, higher auto-ignition temperature, lower heating value, restricted flammability range, low radiation intensity, lower adiabatic flame temperature, and slower chemical conversion rate, all are features that make ammonia a very distinctive fuel [5]. Therefore, a better understanding of ammonia combustion is essential to overcome the limitation of knowledge that bound the behavior of the molecule at various scales.

One of the detriments of ammonia combustion is the production of nitrogen oxides (NO_X). Even though ammonia is carbon-free and can be produced through renewable methods, the combustion products contain NO_X, blend composition, residence time, equivalence ratio, and initial conditions [2, 6–8]. The term NO_X refers to all nitrogen oxides that form from the combustion process, being nitric oxide (NO), nitrogen dioxide (NO_2), and nitrous oxide (N_2O) typically produced in combustion systems. When ammonia is employed, the dominant component of the emitted NO_X is NO. Similarly, NO_2 is the result of NO oxidation processes, being an emission that contributes to acid rain formation [9]. Further, N_2O is considered a very potent greenhouse gas with up to 300 times the Global Warming Potential of carbon dioxide (CO_2) [9, 10]. The formation of nitrogen oxides can be governed by several combustion mechanisms. Ammonia/hydrogen combustion mechanisms have two primary channels. The first includes the fixation process of molecular nitrogen contained in the combustion air (thermal NOx); the other process involves the oxidization of organic nitrogen that is bounded chemically in the fuel (fuel NOx). Figure 1 simply illustrates a layout of the most significant sources of nitrogen oxides in the combustion process.

Much research has been conducted to improve or to find a better understanding of the concept of NO_X formation mechanisms in the combustion of ammonia to develop unique strategies that enable controlling such an emission [11–16]. Recently, fuel NO_X productions from ammonia have been improved with more accurate results for more complex designing applications [17–20], investigate the formation and the reduction of NO_X by developing a unique NH_3 model that covers a wide range of experimental conditions. An oxidation mechanism has been published by [17] which used Shock Tube experiments as a reference. They optimised their work with nine different models to highlight the discrepancies between ammonia kinetic

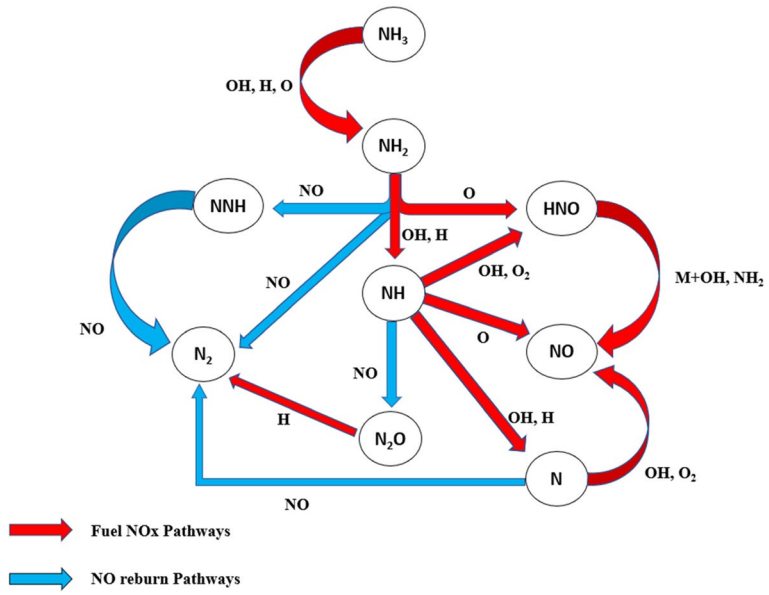

Fig. 1 Reaction pathway diagram illustrating the significant formation/Reburn steps of NO

models. The laminar flame speed has also been investigated in vast research [21] used a cylinder combustion chamber to undertake some measurements related to laminar burning velocity. They used ammonia-air blends under elevated pressure. In this study, the data has been compared with five kinetic mechanisms that were obtained from the literature and that denoted the discrepancies between models and the lack of agreement between the nitrogen-based reactions occurring with these blends. Glarborg et al. [22] established a model that offers reliable diagnostic for the creation and destruction of NO under a wide range of conditions. Their selected model can predict and deliver data for a great variety of industrial processes. The model of [23] was utilized to study the reaction structure zone and reaction pathways of NO and NO_2 in non-premixed flames. This work found a high level of NO concentration in the high-temperature zone, particularly at stoichiometry. Also, the concentration of NO_2 dominated under lean conditions rather than under stoichiometry, where it was found that the level of NO_2 is quite small. The study indicated that the most influential reaction for NO_2 production is $NO + HO_2 = NO_2 + H$, hence reflecting the reason behind the low level of NO_2 at high temperatures. Klippenstein et al. [24] have been conducting their simulations at elevated pressure on the production of prompt NO for premixed flames. The study compared the modeling data with available experimental results and found that high pressure significantly impacts the prompt NO mechanism. Another study has been carried out by [25] to investigate the gas characteristics resulting from a premixed laminar blend of ammonia/air with various equivalence ratios and elevated pressure experimentally and numerically. The study found that both equivalence ratio and pressure affect NO mole fraction.

In conclusion, the complete mechanism for oxidization of intermediates to NO_X is narrow and not fully understood. Due to the lack of information from experimental work, there are still discrepancies in kinetic model predictions, which include uncertainties effect on the thermochemistry and the kinetic rate data. Even though the effort of several researchers by developing NH_3-NO_X kinetic model, a reliable model is not developed yet. Therefore, the present work focuses on studying the concentration of NO and N_2O from the combustion of NH_3/H_2 at 85/15 VOL% at various thermal powers and Reynolds numbers using experimental and numerical tools. This particular blend is unique, as it can potentially enable the use of some doping whilst ensuring reduced ammonia cracking to recover the doping agent (hydrogen). The work is done using a bespoke combustor, whilst the numerical analyses are conducted by employing seven chemical kinetic mechanisms.

2 Methodology

2.1 Experimental work

A burner with a tangential swirl and a geometric swirl number of $S_g = 1.05$ was used in this work at different Re and thermal powers, as illustrated in Fig. 2. A network of Bronkhorst mass flow controllers was utilized to feed the system with flows within 15—95% of the full capabilities with an accuracy of ± 0.5% Rd. The unit has been fed using a blended fuel of ammonia and hydrogen, as mentioned in Table 1. The ammonia and air were introduced via a mixing chamber, while hydrogen was fed through 6 holes with an equal slot. The holes are angled at 45○ and positioned 4 cm below the burner exit. When the hydrogen is injected, it will go directly into the swirl for premixing with ammonia and air. A CH_4 continuous pilot flame was used for ignition and to ignite the flame and kept on to avoid flame extinctions during instability. Along with that, the pilot flame is located above the sampling point to avoid interference with the emissions data. Different conditions were carried out to assess and determine the influence of ammonia concentration on NO_X formation at a constant equivalence ratio.

All the experiments reported here were carried out at atmospheric pressure (~ 1.1 bar) and temperature (~ 288 K) conditions. A pair of LaVision intensified CCD Cameras was employed to examine chemiluminescence traces of several species. The devices were activated simultaneously at 10 Hz and with a gain of 90%. Several Edmond filters were employed for different species, namely, OH* (309 nm) [26], NH* (336 nm) [26–28], and NH2* (630 nm) [26–30]. Five hundred frames per flame have been obtained by using Lavision Davis V10. The frames were post-processed employing a bespoke MatLab script [31], which was designed to undertake Abel Deconvolution after obtaining 3 × 3-pixel median filters and temporary averaging of the 500 images. Five thermocouples have been employed for determining the temperature at five certain points, as illustrated in Fig. 3. The thermocouples with 3 mm diameter were k-type and used in locations 1,4, and 5, while the other thermocouples, 5.60 mm and 10.23 mm diameters were Ceramic shielded R type, and have positioned in locations 3 and 4, respectively. Location 2 was chosen to monitor the flame temperature at the centerline of the flame at 3.9 cm from the quartz exit, while locations 3 and 4 were selected at the same height to monitor the temperature difference at the liner, thus calculating estimated heat loss. Location 1 and 5 were chosen to monitor temperature at the quartz exit liner and burner nozzle wall, respectively. The thermocouples were

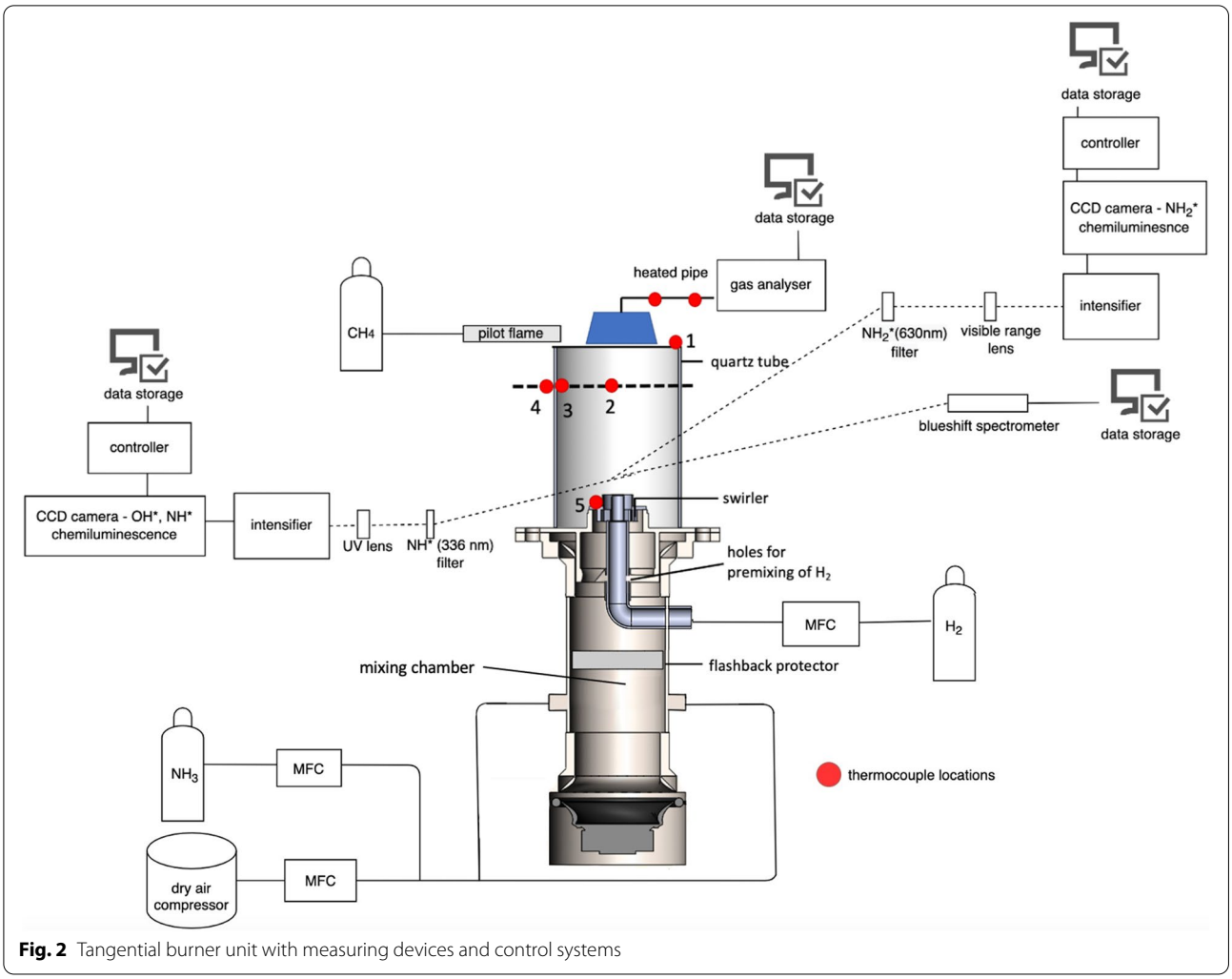

Fig. 2 Tangential burner unit with measuring devices and control systems

directly plugged into a RS data logger and linked to a computer. The calibration process was done previously for the thermocouples, which showed an average error of 3%. The thermocouples measurements have been corrected, taking into consideration the surrounding convective and radiative heat transfer of the thermocouple by implementing Eq. (1), [32].

$$T_g = T_{tc} + \varepsilon_{tc}\sigma\left(T_{tc}^4 - T_w^4\right)\frac{d}{kNu} \quad (1)$$

where T_g is the gas temperature; T_{tc} is the thermocouple bead temperature; T_w is the characteristic radiant surrounding temperature (wall temperature); K is the gas thermal conductivity; ε_{tc} is the emissivity of the thermocouple and Nu is the Nusselt number.

A bespoke Emerson CT5100 quantum Cascade laser analyzer was used to measure several species of interest produced from the combustion process, such as NO, N_2O, NO_2, NH_3, H_2O and O_2. the measurement was undertaken at a frequency of 1 Hz, linearity of

Table 1 Experimental measurements

Parameter	Value	Parameter	Value
Blends NH3/H2 (vol %)	85/15	Inlet Temperature	288 K
Thermal Power	10 kW, 15 kW and 20 kW	Inlet Pressure	0.11 MPa
Reynolds No	20,000, 30,000 and 40,000	Outlet Pressure	0.10 MPa
Equivalence Ratio (Φ)	0.65	Swirl	1.05

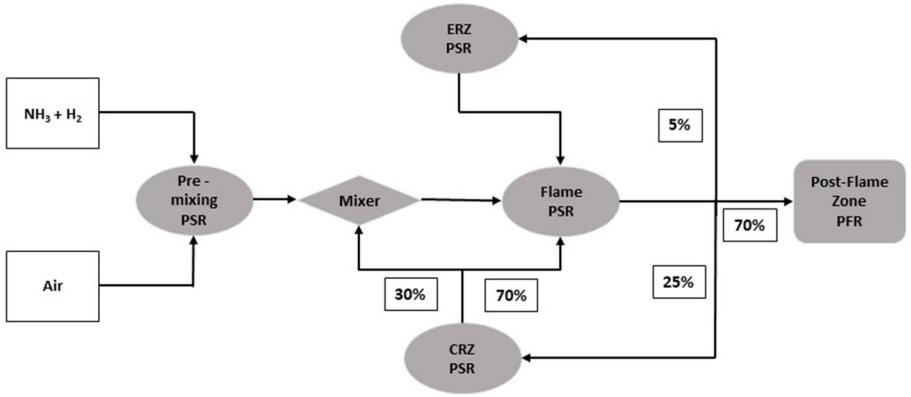

Fig. 3 Chemical reactor network (CRN). CRZ: Central Recirculation Zone; ERZ: External Recirculation Zone

0.999, ± 1% repeatability and 190 °C of sampling temperature. The dilution process was carried out via adding N_2 within the sample with ± 10% repeatability, which was conducted when the wet reading crossed the range of the analyzer detection. A period of 120 s was allocated to do the recording of emission data for each points and to calculate the average for each condition. The flame stability was monitored by using a webcam type Logitech C270, which was installed 5 m away from the burner.

Finally, A UV/visible-capable optical fiber head (Stellernet Inc DLENS with F600 fiber optic cable) was installed 3 cm above the burner's exit and 10 cm away from its central axis. The other end of the optical fiber was connected to a UV/visible-capable spectrometer (Stellernet Inc BLUE-Wave) featuring a 100-mm focal length and a 25-µm wide entry slit. The spectrometer was equipped with a 600-grooves/mm grating and a Si-CCD detector (Sony ILX511b) featuring 2048 effective pixels of size $14 \times 200\ \mu m^2$, yielding a spectral resolution of 0.5 nm. The detector's exposure time was set to 1 s and 20 scans were averaged to improve the signal-to-noise ratio (SNR). The Y-axis of the spectrometer was calibrated using a standard light source (SL1 Tungsten Halogen). In this study, contributions from different species, or specific spectral ranges, were quantified by integration of the chemiluminescence spectra over some specified wavelength ranges. These ranges are 221–261 nm for NO*, 302–326 nm for OH*, 335–346 nm for NH*, and 622–642 nm for NH_2*.

2.2 Chemical kinetic modeling

In the present study, Ansys CHEMKIN-Pro [33] was applied for all numerical simulations to calculate the concentration of NOX emissions. Based on the previous studies [31, 34–36], a chemical reactor network (CRN) was improved for better predictions of emissions from the combustion zone, as illustrated in Fig. 3. The modeling process of Mixing zones, Flame zones, central recirculation zone (CRZ), and external recirculation zone (ERZ) were imitated and modeled using a perfectly stirred reactor (PSR). Residence times were obtained from results obtained during previous numerical validated campaigns [37], delivering values close to 0.05 s at the central recirculation zone and 0.005 s at the shearing flow, with an estimated recirculation of species derived from the previous experimental campaigns [31, 38] as shown in Fig. 3, within the constant volume of the combustion chamber. Although it is emphasized that these numbers are condition dependent (i.e., power, flow, temperature and pressure), their use in previous analyses have delivered acceptable results for the study of various ammonia blends [34]. Thus, they have been also used in this study. As displayed in Fig. 3, The numbers 30% and 70% stand for the volumetric split ratio of the gas supplied to the mixer and flame zone, respectively. While 5%, 25%, and 70% refer to the gas percentages in the external recirculation zone (ERZ), central recirculation zone (CRZ), and post flame zone after the gas crossing the flame zone. Depending on the thermocouple measurements, the approximation of heat loss data has been derived experimentally. The plug flow reactor (PFR) was employed for modeling the post-flame zone with a one-dimensional length of 15 cm, Table 2. The objective of kinetic modelling is to understand the discrepancy between models and identify the most sensitive reactions to the production of NO and N_2O.

Table 2 Grid properties adopted in the current work

Number of grid points	2000
Adaptive grid control of solution gradient	0.02
Adaptive grid control of solution curvature	0.02
Starting axial position	0 cm

2.3 The investigated kinetic models

Seven kinetic reaction mechanisms, published in the past two years including NO_x combustion chemistry suited, were selected to compare the numerical data with experimental measurements for the combustion of the NH_3-H_2 blend. In the following, the kinetic models will be pointed to by a short name representing the first author followed by the year of publication. The kinetic mechanisms are detailed in Table 3 in terms of the number of reactions, the number of species, and the fuel mixture used in each model, as well as the target factors and describe the effects of parameters in the combustion characteristics of each model. The mentioned chemical kinetic mechanisms were selected for sensitivity analysis of reactions and to check the accuracy of the NO_X sub-mechanisms that were newly added to their database depending on previous numerical and experimental campaigns and further validation using a chemical reaction network.

Bertolino et al. [39] adopted a method with a hierarchical and systematic procedure to improve the nominal model of [43] by considering all the target datasets and uncertain parameters. a cumulative impact function (CIF) and Evolutionary Algorithm have been introduced to select the reactions with major impact and to optimize the solution. Their methodology has been supported by using a database of 635 experimental data points that cover ignition delay times, speciation, and laminar burning velocity of ammonia combustion.

Mei et al. [40] introduced a kinetic model for combustion of NH_3/NO at atmospheric conditions (P = 1 atm and T = 298 K) with various equivalence ratios. the model has been improved based on the model reported from [18]. the rate constants of key chemical reactions have been updated, especially those which are directly or indirectly implicated in the interactivity between NH_3 and NO such as $NH_2 + NO = NNH + OH$, $NNH = N_2 + H$, $NNH + NO = N_2 + HNO$ and $NH_2 + NO = N_2 + H_2O$. The kinetic model can offer accurate targets of sensitivity validation for the kinetics of NH_3 and NO interaction.

Han et al. [41] investigated the effect of N_2O enrichment in fuel on the combustion characteristics of NH_3. The impact of rate constants for the most sensitive reactions in ammonia self-ignition and flame propagation of $NH_3 + O_2$ and $H_2 + N_2O$ blends were considered in the study. Their detailed model has been improved based on [46, 47]. The thermodynamic data of nitrogen-based species have been selected from the database of Burcat and Rusicc [48]. while the rate constant of the kinetic reaction $N_2 + O = NO + N$ was considered based on the experimental and kinetic modeling investigation of NO formation in $CH_4 + O_2 + N_2$ premixed flames [48]. Their model has been validated experimentally using the heat flux method at 1 atm and 298 K and the entire range of equivalence ratio.

Zhang et al. [42] constructed a kinetic model which deals with NH_3 and NH_3-H_2 combustion. The model was

Table 3 Chemical kinetic mechanisms used in the present work

No	Kinetic model	No. of Reaction	No. of species	Fuel mixture	Optimization parameter	Parameters effect
1	A.Bertolino et al. [39]	264	38	NH_3	LBVs Ignition delay time speciation measurements	Optimization of nitrogen chemistry based on pressure-dependent reactions
2	B. Mei et al. [40]	264	38	NH_3/NO/N_2	LBVs Markstein length NOx formation	Equivalence ratios
3	X. Han et al. [41]	298	36	NH_3 NH_3/N_2O	LBVs speciation measurements	Equivalence ratios N_2O mixing ratios
4	X. Zhang et al. [42]	263	38	NH_3 NH_3/H_2	NOx formation	Lean and rich conditions Hydrogen-enriched in fuel
5	A. Stagni et al. [43]	203	31	NH_3	LBVs Ignition delay time speciation measurements	Optimization of ammonia oxidation mechanism in a full range of operating conditions
6	X. Han et al. (2019) [44]	130	20	NH_3 + syngas	LBVs Ignition delay time NOx measurements	Equivalence ratios
7	S. de Persis et al. [45]	647	103	CH_4	LBVs NOx measurements	Equivalence ratios Elevated pressure

established based on [18]. The kinetic model has been revisited for the reactions related to NH_3 sub-mechanism. The thermodynamic data of nitrogen-related radicals, especially NH, NH_2, NNH, and N_2H_2, were updated based on the work published by [49]. Also, the rate kinetics of the most important reactions, particularly those related to NO_X formation, have been evaluated based on some experimental [50, 51] and theoretical [43, 49, 52–55] studies. Along with that, the numerical data from model prediction have been validated with JSR experimental measurements of oxidation on NH_3-H_2 blended flames at atmospheric pressure, low -moderate temperatures (800–1280 K), different H_2 contents, 0-70VOL% in the fuel, and various equivalence ratios.

Stagni et al. [43] developed a kinetic model that deals with ammonia oxidation in a wide range based on various studies, including NO_X sub-mechanism from [64], updating the $HONO/HNO_2$ chemistry depending on the work reported by [56], and updating the thermodynamic database of all species depending on [48]. Also, the NH_2OH chemistry and dissociation reaction were considered, particularly for the reactions involving NH and NH_2 radicals from work published by [57]. The capability of the kinetic model has been tested in various configuration systems (Shock tube, Rapid compression machine, Flow reactor, Laminar flame speed, and burner-stabilized flame) and assessed in a wide range of operation conditions.

Han et al. [44] reported a kinetic model that estimates NO_X emissions characteristics for ammonia oxidation. The study of Varga et al. [58] was the starting point for developing their kinetic model. The study included updating the database of constant rate parameters, collision factors, and pressure-dependent coefficients for the most critical reactions in ammonia oxidations, considering the individual investigation option for each reaction and its effect on laminar burning velocity. The role of HONO, HNOH, HON, HNO_2, $HONO_2$, and NO_3 reactions on the combustion characteristics has also been reported. In terms of validation, the model was tested and compared with several experimental measurements from literature with various operation conditions and equivalence ratios.

De Persis et al. [45] developed a kinetic mechanism for predicting nitrogen oxide formation. The effect of both equivalence ratio and pressure on NO mole fractions has been considered. The NO_X sub mechanism has been developed and revised based on the investigation work done by Lamoureux et al. [59]. The contribution of NO major pathways (prompt, thermal, NNH, and N_2O) has been reported and compared with the study from [24]. The mechanism has been validated based on experimental measurements of NO mole fraction profile using the LIF method in laminar counterflow configuration system at various equivalence ratios and pressure ranging from 1 -7 atm.

As shown in Table 3, all the mechanisms improved the NH_3 sub mechanisms in their database with corresponding thermochemistry data. Most of these models directly describe the combustion of NH_3 except de Persis model that deals with CH_4 flames, but it already has a NO_X formation mechanism in its database and improved to some limits to forecasting acceptable levels of NO_X.

The kinetic mechanisms containing nitrogen chemistry in its database would describe the combustion of ammonia. Along with that, the weak performance of these models does not mean the model is not well applicable for the conditions of interest, which it was originally improved for.

3 Results and discussions

In this section, the experimental results are compared with predicted data obtained via detailed kinetic models described in Sect. 2.1. Both experimental and numerical data were carried out in the same conditions of pressure and temperature (NTP). The equivalence ratio for the lean mixture of NH_3/H_2 fuel was kept constant for all cases ($\emptyset = 0.65$).

3.1 Effects of Reynolds number

Constant Reynolds number is one of several essential parameters in investigating the performance of many practical systems, especially power generation and comparison aims between combustion system configurations [60]. To analyze the influence of turbulence factors on the combustion characteristics such as flame and emissions, three values of Reynolds number (20,000, 30,000, and 40,000) will be considered at a fixed equivalence ratio of 0.65. The figures below compare the present NO and N_2O measurements with data estimated from kinetic models and for different Reynolds numbers in the range 20,000–40,000 at combustor exhaust. The mole fractions of NO and N_2O in Figs. 4 and 5 are presented in units of ppmv. As shown in Fig. 4, the mole fraction of NO increases with the Reynolds number. The NO mole fraction resulting via experiments was close to data obtained by Stagni's model. Based on the comparison between the present study results and the modelling data from the literature, both Bertolino's and Stagni's mechanisms have a closer, reasonable agreement with the experimental data.

Figure 5 shows the variation of the mole fraction of N_2O in ppmv when the Reynolds number increases from 20,000 to 40,000 at zone exhaust. Bertolino's, Stagni's, and Bowen Mei Mechanisms gave better estimation to these experimental results than other models.

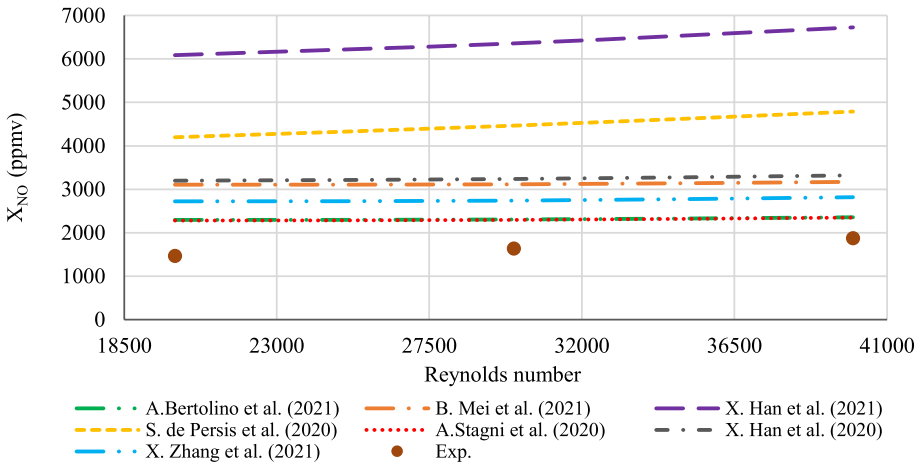

Fig. 4 Comparison between experimental results and numerical concentration profiles of NO when the Reynolds number varies from 20,000 to 40,000 at the exhaust

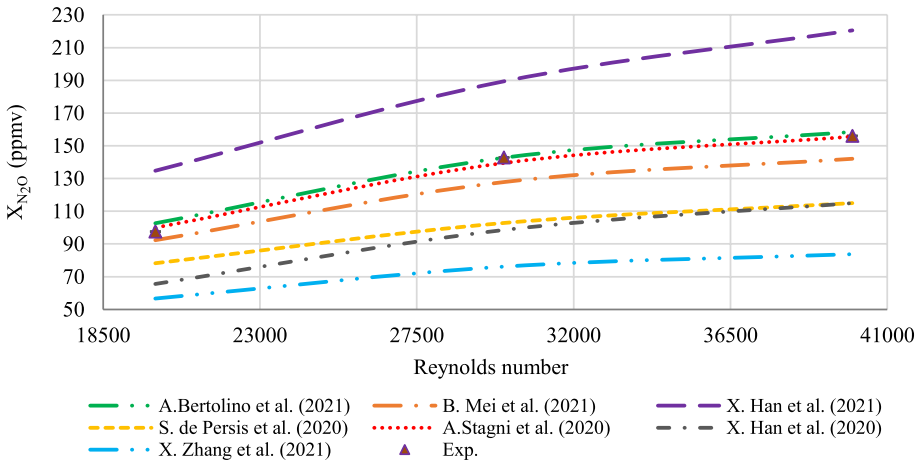

Fig. 5 Comparison between experimental results and numerical concentration profiles of N_2O when the Reynolds number varies from 20,000 to 40,000 at the exhaust

Figures 6 and 7 demonstrate the radical spectroscopic spectrum and the chemiluminescence data, respectively, of different radicals of interest at a constant equivalence ratio of 0.65 and under different Reynolds numbers at the flame zone. The chemiluminescence images of OH*, NH*, and NH_2* in Fig. 7 were normalized to image dataset max to display radicals distributions in the flame. Table 4 shows the integrated intensities of different radicals from the spectrum shown in Fig. 6. As can be seen, the concentration of NO emissions at the exhaust reported minimum level when the Re = 20,000. The reason behind that is the deterioration of the flame characteristics due to lower reactivity and radical formation at Re = 20,000. This behavior can be seen clearly in Fig. 7, the distribution of radicals expands with increasing Re. The integrated radical intensities of NO*, OH*, NH*, and NH_2* in Table 4 shows an increasing trend as Re increased from 20,000 to 40,000 which is also obvious in Fig. 7. It was interesting to notice the increase in radical intensities is much lower when Re increased from 30,000 to 40,000, which reflects into exhaust emissions as well, thereby signifying the importance of these radicals in NH_3/H_2 flames. In Fig. 7, the flame brush expands with increasing Re, giving an indication of an increase in the radical concentrations. The increase in NH_2* radicals with increasing Re is due to OH* radical abundance and its role in the chemical reaction $NH_3 + OH \leftrightarrow H_2O + NH_2$. OH* radicals are also responsible for NH* production through the reaction $NH_2 + OH \leftrightarrow NH + H_2O$ and

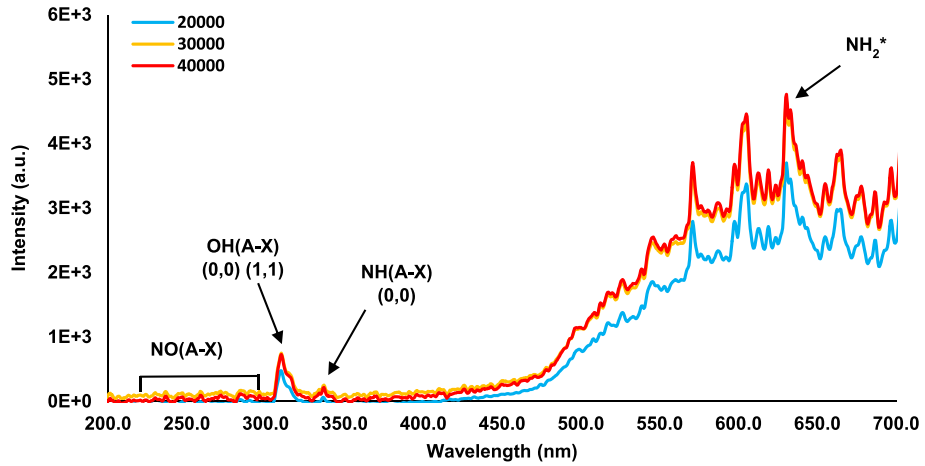

Fig. 6 Chemiluminescence spectrum at Φ = 0.65 and various Reynolds numbers at the flame zone

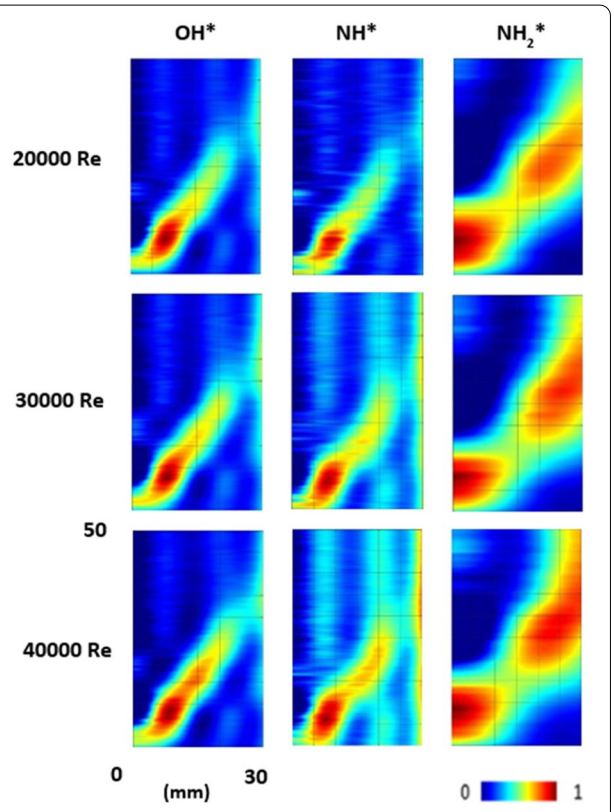

Fig. 7 NH*, NH_2*, and OH* chemiluminescence at 85/15 $_{VOL\%}$ Of NH_3/H_2 blend at Φ = 0.65 and various Reynolds numbers at the flame zone. Colormap normalized to image dataset maximum

Table 4 NO*, OH*, NH* and NH2* values resulted at various Re

RADICALS RANGE	*Re = 20,000*	*Re = 30,000*	*Re = 40,000*
NO* (221—261 nm)	2817	4920	4941
OH* (302—326 nm)	10,258	13,688	14,602
NH* (335—346 nm)	1552	2495	2768
NH2* (622—642 nm)	122,973	151,558	158,137

can be considered the largest source of NH production from NH_2. Eventually, NH* radicals are consumed through the chemical reaction $NH + NO \leftrightarrow N_2O + H$ to form N_2O by consuming NO. The considerable increase in N_2O when Re = 40,000 can be attributed to increased flame temperature, thus higher heat loss through the quartz liner. This phenomenon will be analyzed further in the latter part of the study.

3.2 Effects of thermal power

Figures 8 and 9 illustrate the variation of NO and N_2O concentration in ppmv in terms of thermal power at the exhaust. The figures also include data from seven literature models run under the same operating condition. As can be seen, the mole fractions of NO peaked at 15 kW thermal power. NO mole fraction decreased with the decrease or increase in thermal power from 15 kW. All models predicted similar trends. However, the NO concentration resulting from experiments was close to those predicted by Stagni's, Betrolino's, and Zhang's mechanisms.

Figure 9 shows the concentration of N_2O. The figure illustrates a sharp decay in the concentration of N_2O when the thermal power equals 15 kW. As power was increased to 20 kW, the N_2O mole fraction increased and nearly gave the same value to that of a thermal power equal to 10 kW. Stagni's, Betrolino's, and Bowen Mei's mechanisms achieved a good agreement with the

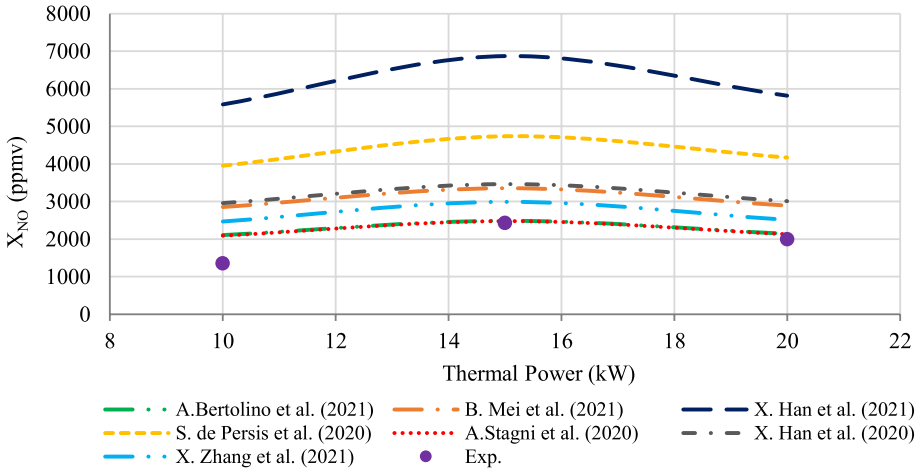

Fig. 8 Comparison between experimental results and numerical concentration profiles of NO when thermal power in rang 10-20kW at the exhaust

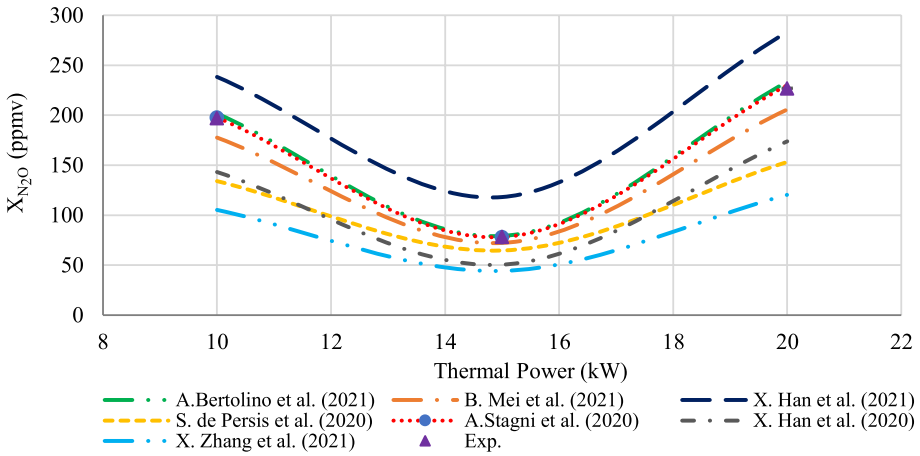

Fig. 9 Comparison between experimental results and numerical concentration profiles of N_2O when thermal power in range 10-20kW at the exhaust

experimental results of the present study. In contrast, the other mechanisms gave the same trend but with a difference in the concentration of N_2O.

The radical spectroscopic spectrum at different thermal power with a constant equivalence ratio of 0.65 at the flame zone is presented in Fig. 10, while Fig. 11 denotes the chemiluminescence imprints of this blend at various powers. Similar to previous discussions, colormaps were normalized to image dataset maximum to show the changes in radicals distributions as thermal power changes. Table 5 provides the integrated intensities of different radicals from Fig. 10. OH*, NH*and NH_2* figures show an increase in their concentration when the thermal power increased up to 15 kW then decreased with increasing thermal intensity to reach 20 kW, Table 5. Simultaneously, this can be appeared clearly, especially when the thermal intensity increases from 10 to 15 kW, the flame brush expands due to increasing the OH*, NH*, and NH_2* radical concentrations, Fig. 11. The increased production of these radicals at 15 kW reflects into increased NO productions and decreased N_2O productions. This is further confirmed by the maximum radical intensity of NO* at 15 kW, Table 5. It is believed that NO production, in this case, is due to the conversion of NH_2 to NH through reactions with OH radicals, then combining NH and OH to form HNO, which is known to be the main source of NO formation in most mechanisms. Simultaneously, the chain branching reaction $NH_2 + NO \leftrightarrow NNH + OH$ and the chain-terminating

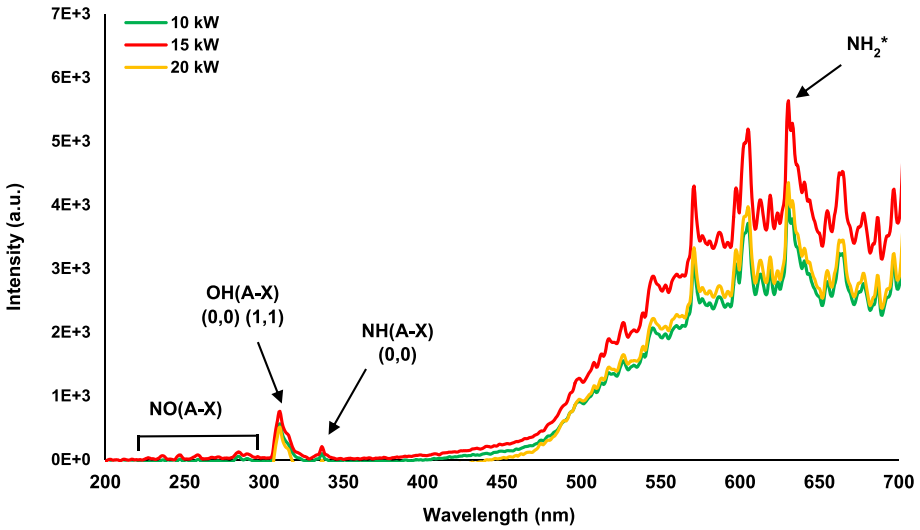

Fig. 10 Chemiluminescence spectrum at Φ = 0.65 and various thermal powers at the flame zone

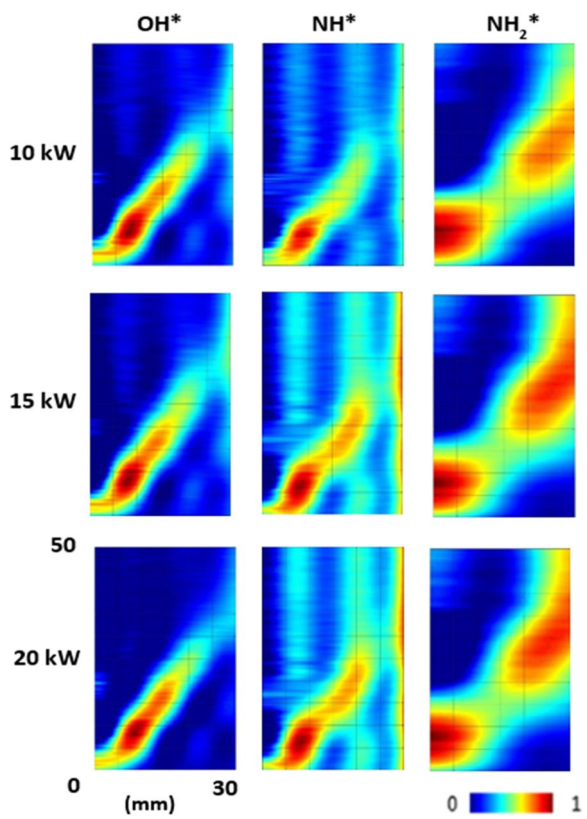

Fig. 11 NH*, NH_2*, and OH* chemiluminescence at 85/15 VOL% Of NH_3/H_2 blend at Φ = 0.65 and various thermal power at the flame zone. Colormap normalized to image dataset maximum

Table 5 NO*, OH*, NH* and NH2* values resulted at various Re

RADICALS RANGE	*10 kW*	*15 kW*	*20 kW*
NO* (221—261 nm)	3108	4720	4468
OH* (302—326 nm)	11,677	15,045	14,039
NH* (335—346 nm)	1687	2503	2405
NH2* (622—642 nm)	134,210	184,198	150,000

reaction $NH_2 + NO \leftrightarrow H_2O + N_2$ are known as the key chain reactions for NO consumptions [34].

3.3 Sensitivity analyses

As can be seen from the concentration profiles for both NO and N_2O in the above figures, Han's mechanism gave the highest over-prediction for NO and N_2O. At the same time, Zhang's mechanism predicts a low concentration of N_2O. Stagni, Betrolino, and Bowen Mei mechanisms are the most accurate models since they predict data near the range of experimental combustion results. Therefore, sensitivity analyses and rate of production for NO and N_2O as well as the NO_X formation/consumption pathways at the flame zone are presented using Stagni, A.Betrolino, and Bowen Mei's kinetic models. As the highest exhaust emissions were observed at high thermal power, 20 kW, and high Reynolds number, 40,000, these conditions have been selected for analyzing the sensitivity and rate of production of both NO and N_2O species in this part of the study.

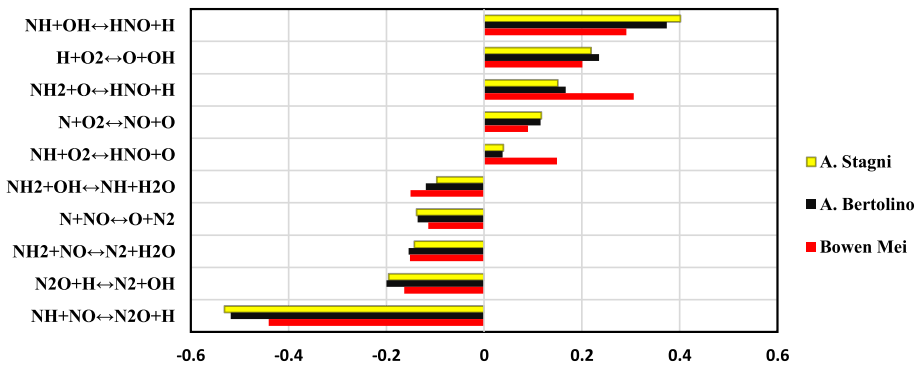

Fig. 12 Sensitivity analysis diagram of NO at the flame zone for 20 kW thermal power

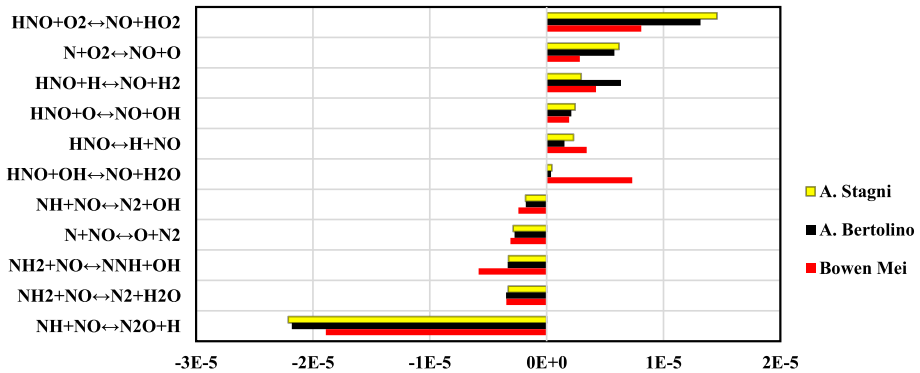

Fig. 13 Rate of production diagram of NO at the flame zone for 20 kW thermal power

3.4 [NO] Sensitivity analysis

NO is one of the most critical ammonia combustion products since it has a dangerous effect on the ecosystem with the production of acid rain and other environmental impacts. To study NO's chemistry and investigate the contribution of NO in the formation of N_2O, sensitivity analyses have been considered for two previously explained conditions in this part of the study.

3.4.1 [NO] Sensitivity analysis for 20 kW of thermal power

Figures 12, 13 and 14 depict the sensitivity analysis of NO, rate of production, and NO formation/decomposition pathways, respectively, at the combustion flame zone when thermal power is equal to 20 kW using three kinetic models. As can be seen from the pathway's diagram, HNO shows a great tendency to form NO at the flame zone and can be considered the primary source of NO production.

From Fig. 12, all the kinetic models show high positive sensitivity for the reaction $NH + OH \leftrightarrow HNO + H$, and this reaction is considered the most influential reaction in producing HNO species, among other reactions. Also, the high positive sensitivity of the reaction $H + O_2 \leftrightarrow O + OH$ leads to an increase in the possibility of the formation of HNO through the reactions $NH_2 + O \leftrightarrow HNO + H$ and $NH + OH \leftrightarrow HNO + H$ due to the abundance of O and OH radicals.

As can be seen from Fig. 13, Stagni and Bertolino's models indicate that the most prominent chemical reactions responsible for NO production from HNO are $HNO + O_2 \leftrightarrow NO + HO_2$ and $HNO + H \leftrightarrow NO + H_2$. At the same time, the Bowen Mei mechanism illustrates that both reactions $HNO + O_2 \leftrightarrow NO + HO_2$ and $HNO + OH \leftrightarrow NO + H_2O$ are the most effective in producing NO from HNO. Most importantly, the chemical reaction $NH + NO \leftrightarrow N_2O + H$ is responsible for consuming the NO and transforming it to N_2O by reacting with NH. All three mechanisms indicate that $NH + NO \leftrightarrow N_2O + H$ is the dominant reaction in consuming NO, among other reactions.

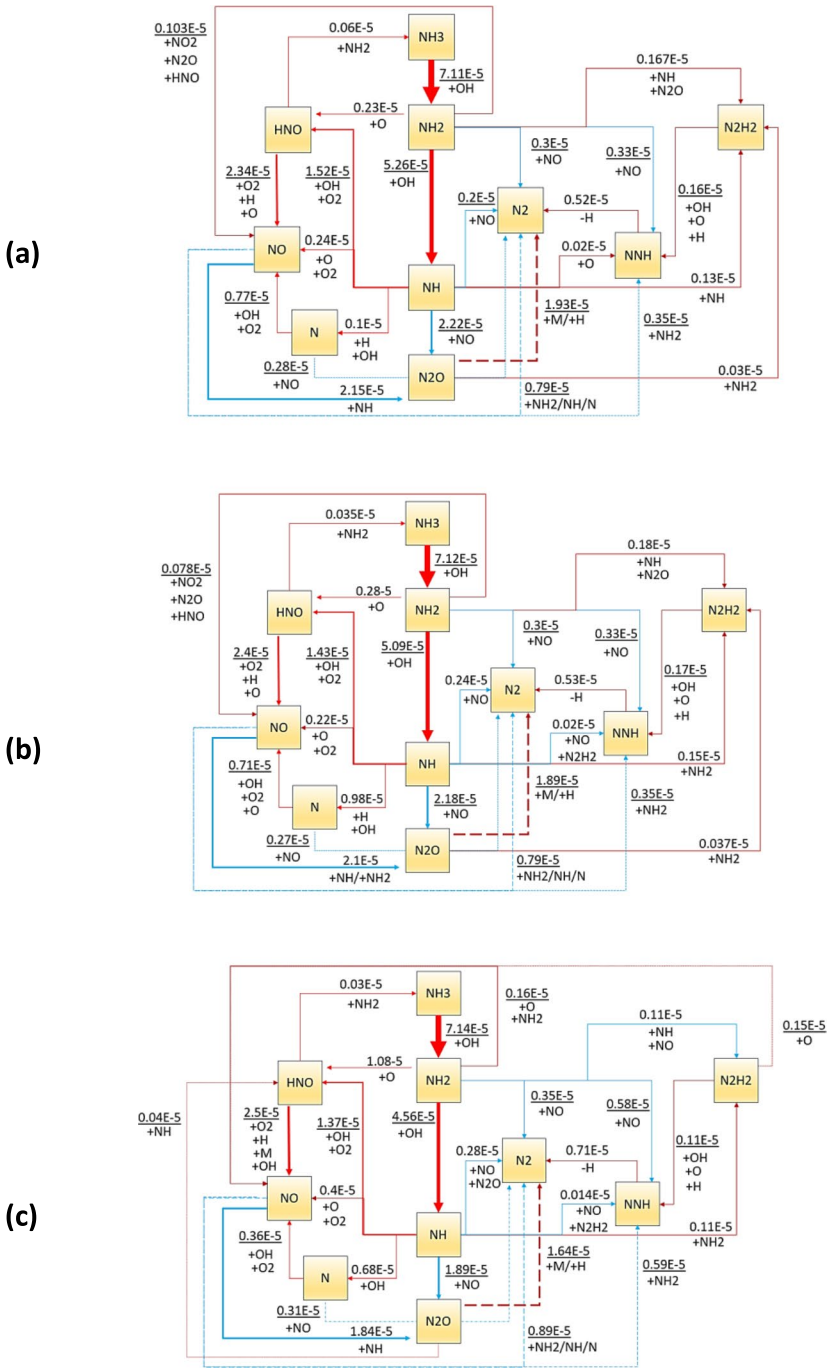

Fig. 14 Chemical reaction pathways show NO_X formation/consumption at flame zone when thermal power equal to 20 kW predicted by (**a**) Stagni, (**b**) Bertolino, and (**c**) Mei kinetic models. Lines refer to the reaction path; Numbers stand for the absolute rate of production in ppmv, which has been represented by line thickness for better explanation

As shown from Fig. 14, the pathway diagrams predicted from all three kinetic models indicate that NH_2, NH, and N radicals tend to react with NO to produce N_2 but at different concentrations. Also, the substantial contribution of both chemical reactions, $NH_2 + NO \leftrightarrow NNH + OH$ and $NH_2 + NO \leftrightarrow N_2 + H_2O$ for converting NO to NNH and N_2, respectively, can be noticed in all three kinetic mechanisms. Along with that, the Bowen Mei mechanism shows a considerable increase in the amount of NO reacting with NH_2 to produce NNH through the chemical reaction $NH_2 + NO \leftrightarrow NNH + OH$, and with NH_2, NH and N by $NH_2 + NO \leftrightarrow N_2 + H_2O$, $NH + NO \leftrightarrow N_2 + OH$ and $N + NO \leftrightarrow O + N_2$, compared to the other kinetic mechanisms considered here which demonstrate lower reacting concentrations of NO to produce NNH and N_2.

3.4.2 [NO] Sensitivity analysis when Re = 40,000

Figures 15, 16 and 17 show the sensitivity analysis, the rate of production, and formation/destruction pathways for NO, respectively, using the three kinetic models when Reynolds number equals 40,000.

As can be seen from the pathway's diagram N, NH, NH_2, and HNO are the species responsible for NO formation at the flame zone. As seen earlier, HNO has a significant effect on the formation of NO and can be considered the dominant source of NO production among other species. In addition, the effect of Reynolds number was considerably noticed as the concentration of NO from HNO increased noticeably compared to NO-pathways from Fig. 14 for Stagni and Bertolino. At the same time, the Bowen Mei mechanism demonstrates a different effect, as the NO concentration is reduced and shows the role of the N_2H_2 in the formation of NO.

Figure 15 illustrates NO sensitivity analysis at the flame zone when Reynolds number hit 40,000. The sensitivity level of the reaction $H + O_2 \leftrightarrow O + OH$ is high and gives a positive value to produce O and OH radicals. The abundance of O and OH radicals encourage the reactions $NH + OH \leftrightarrow HNO + H$ and $NH_2 + O \leftrightarrow HNO + H$ in the formation of HNO which is the main source of NO formation as these reactions show high positive sensitivities of HNO formation.

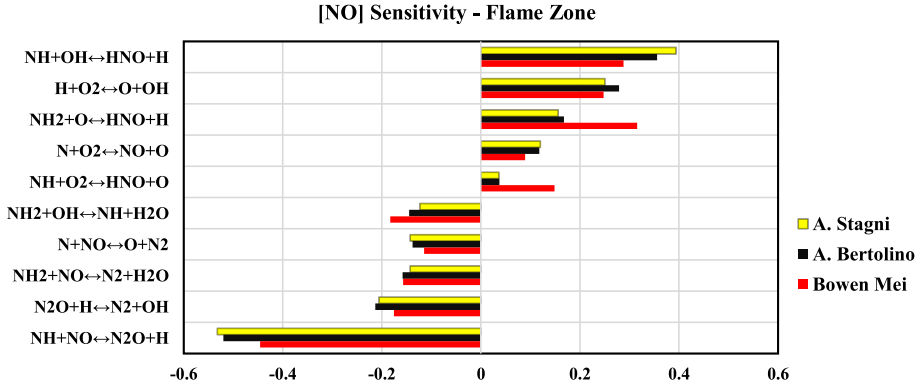

Fig. 15 Sensitivity analysis diagram of NO at flame zone when Reynolds number equal to 40,000

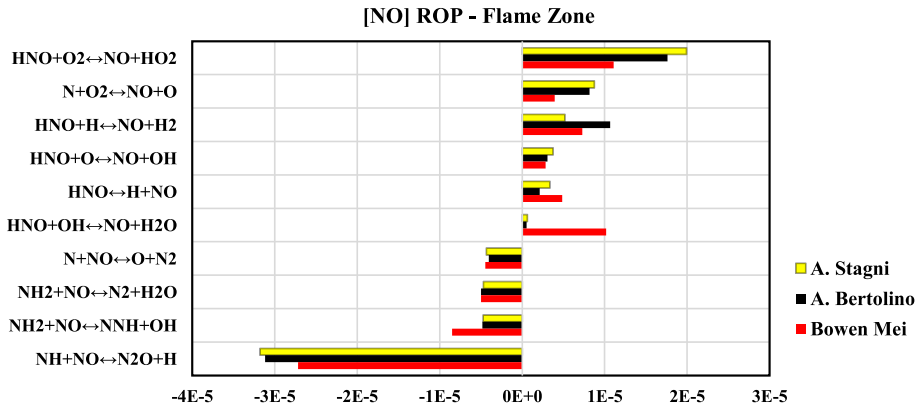

Fig. 16 Rate of production diagram of NO at flame zone when Reynolds number equal to 40,000

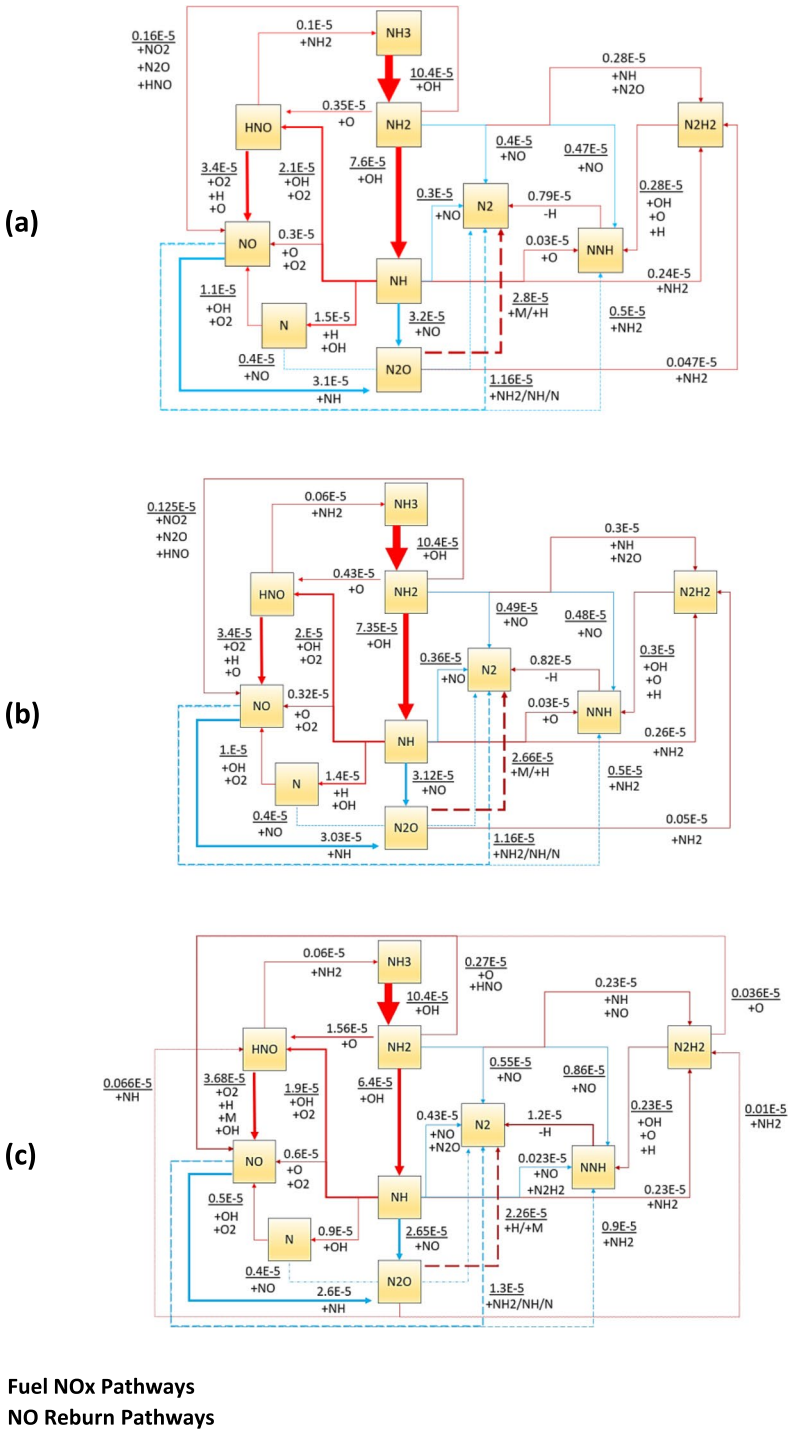

Fig. 17 Chemical reaction pathways presenting NOx formation/ consumption at flame zone, Reynolds number equal to 40000 predicted by (**a**) Stagni, (**b**) Bertolino, and (**c**) Mei kinetic models.: Lines refer to the reaction path; Numbers stand for the absolute rate of production in ppmv, which has been represented by line thickness for better explanation

Figure 16 shows NO production rates and illustrates that the dominant chemical reactions for the creation of NO are $HNO + O_2 \leftrightarrow NO + HO_2$ and $N + O_2 \leftrightarrow NO + O$ for both Stagni and Bertolino models. However, the Bowen Mei mechanism predicts that NO could be produced due to

the reaction of HNO with O_2 and OH through the reactions $HNO + O_2 \leftrightarrow NO + HO_2$, and $HNO + OH \leftrightarrow NO + H_2O$, respectively, and can be considered the controlling reactions responsible for NO formation. In addition to that, the chemical reaction $NH + NO \leftrightarrow N_2O + H$ gives a negative rate of NO production for all three kinetic mechanisms.

As can be noticed from Fig. 17, the pathway's layout indicates the consumption of NO is dependent on the availability of NH_2, NH, and N radicals to react with NO. All three mechanisms give similar trends but with different concentrations since the chemical reactions $NH_2 + NO \leftrightarrow NNH + OH$ and $NH_2 + NO \leftrightarrow N_2 + H_2O$ are responsible for consuming NO to form NNH and N_2. Further, the pathway's diagram clearly shows the effect of Reynolds number on NH_3, NH_2, and NH compared to the thermal power pathway's diagram (Fig. 14). It shows an increase in the reactive amount of NH_3 with OH to produce NH_2, a similar effect that occurs with NH_2 and NH for all three models. The Bowen Mei mechanism clearly indicates the role of N_2H_2 in the formation of NO compared with Stagni and Bertolino, as the reaction is not included in their predicted pathway diagram.

3.5 [N_2O] Sensitivity analysis

One of the most important drawbacks of ammonia combustion could be N_2O, especially under lean conditions. The gas has a much greater Global Warming Potential than CO_2. Hence, it is important to determine its sensitivity analyses, rates of production of various species and to create a pathway's diagram to examine the role of N_2O in the ammonia combustion process in two conditions previously discussed.

3.5.1 [N_2O] Sensitivity analysis for 20 kW of thermal power

Figures 18 and 19 show the sensitivity analysis and rate of production of N_2O using the three kinetic mechanisms when the thermal power is equal to 20 kW. It has been noticed that the chemical reaction $NH + NO \leftrightarrow N_2O + H$ has a considerable effect on the formation of N_2O. Along with that, $NH_2 + OH \leftrightarrow NH + H_2O$ and $H + O_2 \leftrightarrow O + OH$ also participate in the creation of N_2O. All three mechanisms give nearly the same trend for N_2O concentration. In addition, the Bowen Mei mechanism shows that the N_2O formation rate is higher than that predicted by Stagni and Bertolino kinetic models. The chemical reaction $N_2O + H \leftrightarrow N_2 + OH$ gives a pessimistic sensitivity prediction for N_2O, which can be observed

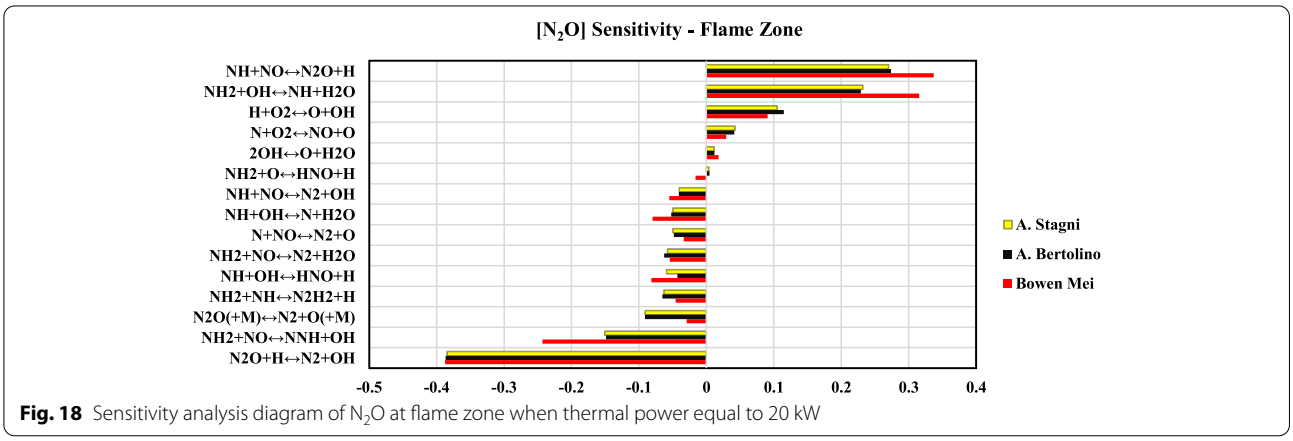

Fig. 18 Sensitivity analysis diagram of N_2O at flame zone when thermal power equal to 20 kW

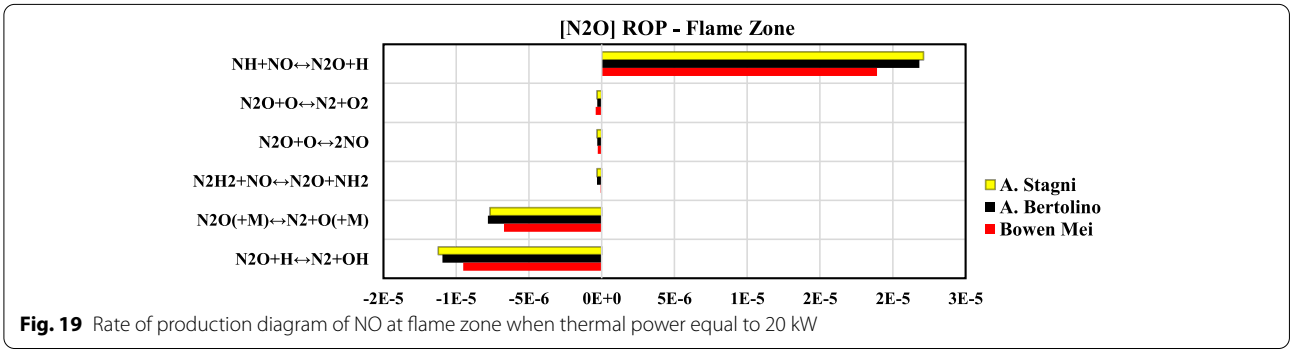

Fig. 19 Rate of production diagram of NO at flame zone when thermal power equal to 20 kW

for all three kinetic models. In Fig. 19, the third body reaction $N2O(+M) \leftrightarrow N2 + O(+M)$ showed a negative production rate for N_2O in all three models.

The pathways diagram from Fig. 17 indicates that both NH and NO are the major sources for the formation of N_2O. NO reacts with NH radicals through the chemical reaction $NH + NO \leftrightarrow N_2O + H$ to produce N_2O. At the same time, Both Stagni and Bertolino's chemical models predict the consumption path of N_2O to N_2 via the chemical reactions $N_2O + H \leftrightarrow N_2 + OH$ and the decomposition path of N_2O through the chemical reaction $N_2O + NH_2 \leftrightarrow N_2H_2 + NO$. In comparison, the Bowen Mei mechanism indicates that $N_2O + NH \leftrightarrow HNO + N_2$ is also responsible for consuming N_2O to produce HNO, and this reaction does not appear in Stagni and Bertolino models. All three models indicate that the reaction $N_2O + H \leftrightarrow N_2 + OH$ is substantial in consuming N_2O to N_2.

3.5.2 [N_2O] Sensitivity analysis when Re = 40,000

Figures 20 and 21 refer to the sensitivity analysis and rate of production of N_2O at operational conditions at Re = 40,000. Figure 20 shows that both reactions $NH + NO \leftrightarrow N_2O + H$ and $NH_2 + OH \leftrightarrow NH + H_2O$ have a positive sensitivity for all three models. Along with that, the Bowen Mei model gives higher predictions to both previous chemical reactions compared with Stagni and Bertolino models. In addition, $NH_2 + NO \leftrightarrow NNH + OH$ and $N_2O + H \leftrightarrow N_2 + OH$ give negative sensitivity of N_2O for all three models, whilst the Bowen Mei mechanism also predicts a high negative sensitivity level of $NH_2 + NO \leftrightarrow NNH + OH$ in comparison to Stagni and Bertolino kinetic mechanisms.

Figure 21 indicates that $NH + NO \leftrightarrow N_2O + H$ is one of the dominant reactions for the formation of the pollutant. Further, the third body reaction $N_2O(+M) \leftrightarrow N_2 + O(+M)$ and $N_2O + H \leftrightarrow N_2 + OH$ present negative rates of production that lead to a decrease in the concentration of N_2O. Also, all three mechanisms indicate that the chemical reaction $N_2O + H \leftrightarrow N_2 + OH$ is mainly responsible for the consumption of N_2O.

As can be seen from Fig. 17, Stagni and Bertolino's models predict the formation of N_2O due to the chemical reaction $NH + NO \leftrightarrow N_2O + H$. Stagni and Bertolin models identify small amounts of N_2O consumptions via the reaction with N_2 and N_2H_2 with the radicals H and NO, respectively. However, the Bowen Mei mechanism

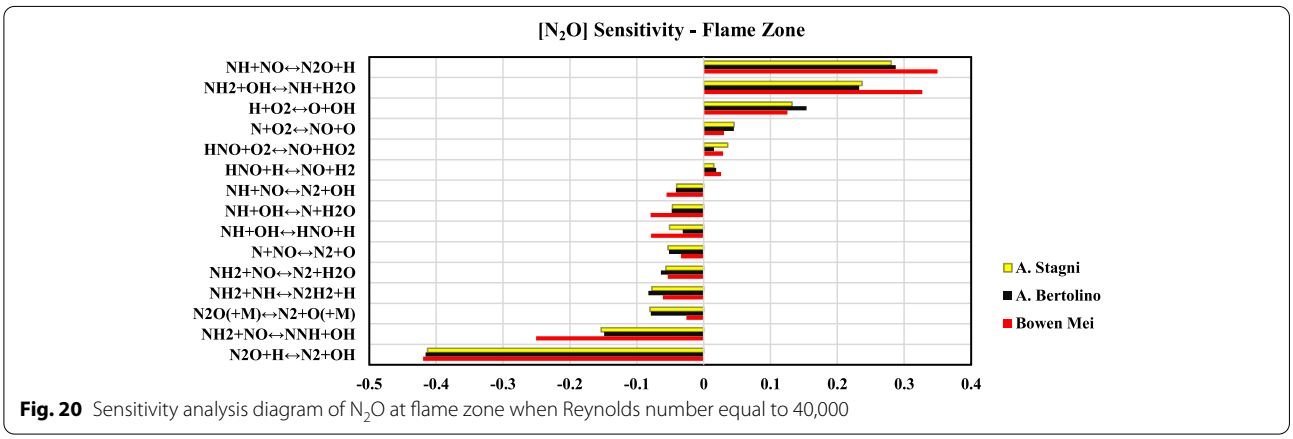

Fig. 20 Sensitivity analysis diagram of N_2O at flame zone when Reynolds number equal to 40,000

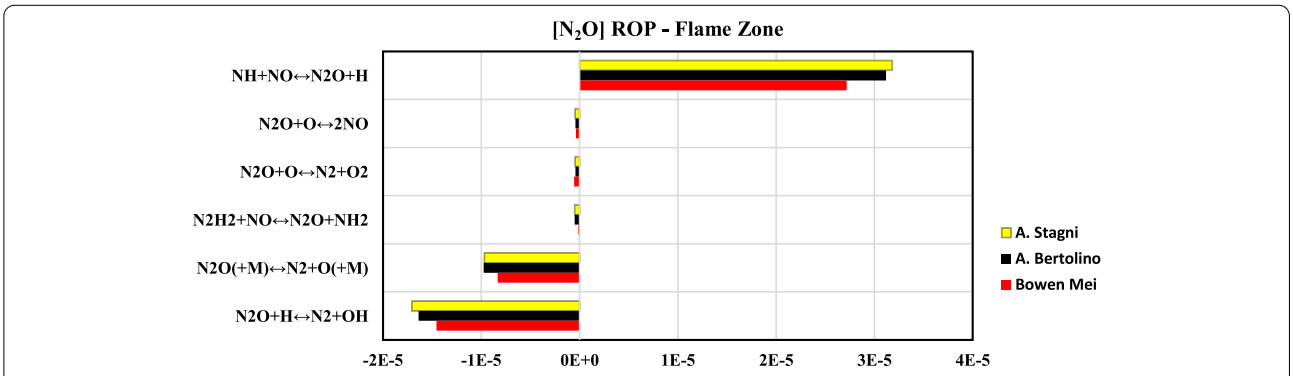

Fig. 21 Rate of production diagram of N_2O at flame zone when Reynolds number equal to 40,000

denotes NH radical's role in producing HNO through the reaction $NH + N_2O \leftrightarrow N_2 + HNO$ along with other reactions mentioned in the other models for the consumption of the species. From an operational condition perspective, the pathways diagram for both cases shows that Reynolds number has an obvious effect in increasing the concentration of N_2O compared to thermal power. The Reynolds number effect extends to the consumption side of N_2O; all the models demonstrate an increase in the consumption rate of N_2O, thus producing N_2 and N_2H_2. Even though there are differences in the final concentrations of N_2O, all the kinetic mechanisms gave similar trends.

4 Conclusions

The present work has investigated the concentrations of NO and N_2O at 85/15 (%vol) of NH_3/H_2 blend using both experimental and numerical analyses. Experiments at various Reynolds numbers and thermal powers have been carried out at standard atmospheric conditions (1.1 bar and 288 K). The experimental results have been used to validate the numerical data and check the accuracy of kinetic models adopted in this study. Seven recently published kinetic models for ammonia combustion have been used and showed different predictions. The kinetic mechanisms of Stagni et al. and Bertolino et al. have given the best agreement in the prediction of NO and N_2O over various thermal powers and Reynolds numbers. The main conclusions of this study can be summarized as follows.

- Measurements in terms of thermal power: The maximum concentration of NO is when the thermal intensity reaches 15 kW and then decreases for other cases, while the N_2O mole fraction reaches a peak when the thermal power is equal to 20 kW, and its concentration decreases to record a minimum value at 15 kW. Along with that, the numerical investigation showed that $HNO + O_2 \leftrightarrow NO + HO_2$, $N + O_2 \leftrightarrow NO + O$, and $HNO + H \leftrightarrow NO + H_2$ are the most critical reactions for NO formation at 20 kW. In addition, the chemical reaction $NH_2 + OH \leftrightarrow NH + H_2O$, $H + O_2 \leftrightarrow O + OH$, and $NH + NO \leftrightarrow N_2O + H$ substantially affect the formation of N_2O.
- Measurements in terms of Reynolds number: the NO productions increased gradually when the Reynolds number varied from 20,000 to 40,000 and recorded a maximum value at Re = 40,000. The same behavior was noticed with N_2O, as the concentration of N_2O reaches the maximum at the maximum Re (40,000). Also, the NH and NO radicals when Re = 40,000 are more than those resulting in other Re values. The reason behind this effect is that NO heavily participates in the formation of N_2O. Further, the numerical analyses for Stagni and Bertolino kinetic models depicted that the dominant reactions behind the formation of NO were $HNO + O_2 \leftrightarrow NO + HO_2$ and $N + O_2 \leftrightarrow NO + O$, which differed from those in the Bowen Mei et al. [40] model. Also, the Bowen Mei model predicted high sensitivity values for $NH + NO \leftrightarrow N_2O + H$ and $NH_2 + OH \leftrightarrow NH + H_2O$, which play an essential role in the formation of N_2O, different from Stagni and Bertolino assumptions.

The impact of Reynolds number and thermal intensity conditions on the N_2O and NO emissions level has been clearly shown. Therefore, the intensity of produced radicals such as NH*, NH_2*, and NO* increased with varying Reynolds conditions from 20,000 to 40,000, whereas peaks of the radicals were noticed at 15 kW thermal power. Finally, a considerable amount of NO is consumed by reactions with NH to produce N_2O through the chemical reaction $NH+NO \leftrightarrow N_2O+H$, a behavior that intensifies when Re =40,000.

Abbreviations

NH_3: Ammonia; H_2: Hydrogen; NO: Nitrogen monoxide; NO_2: Nitrogen Dioxide; N_2O: Nitrous oxide; N_2: Nitrogen; NO_X: Nitrogen oxides; CO_2: Carbon dioxide; NH, NH_2: Nitrogen hydrides; OH: Hydroxide; Re: Reynolds Number; NTP: Normal pressure and temperature; CRZ: Central Recirculation Zone; ERZ: Eternal recirculation zone.; G: Gas; Tc: Thermocouple; w: Wall; *: Radical.

Authors' contributions

Conceptualization—Alnasif A. and Mashruk S.; Investigation—Mashruk S., and Alnasif A.; Methodology—Valera-Medina A, Mashruk S., and Alnasif A; Project administration—Valera-Medina A, Mashruk S.; Resources—Valera-Medina A., Mashruk S., and Alnasif A.; Supervision—Valera-Medina A.; Visualization—Alnasif A. and Mashruk S.; Writing—original draft—Alnasif A. and Mashruk S.; Writing—review and editing—Mashruk S., Kovaleva M., Wang P., and Valera-Medina A. All authors have read and agreed to the published version of the manuscript.

Funding

This work was supported by the SAFE-AGT pilot (no. EP/T009314/1) with funding from the Engineering and Physical Sciences Research Council (EPSRC). The research was undertaken at Cardiff University's Thermofluids Lab (W/0.07) with invaluable technical support from Mr. Malcolm Seaborne. Engineering and Physical Sciences Research Council,EP/T009314/1,A Valera-Medina

Availability of data and materials

Information on the data underpinning the results presented here, including how to access them, can be found in the Cardiff University data catalogue at http://orca.cf.ac.uk/XXXXXX.

Declarations

Competing interests

The authors declare no conflict of interest.

Author details

[1]College of Physical Sciences and Engineering, Queen's Building, Cardiff University, Cardiff, Wales CF243AA, UK. [2]Engineering Technical College of Al-Najaf, Al-Furat Al-Awsat Technical University, Najaf 31001, Iraq. [3]Institute for Energy Research, Jiangsu University, Jiangsu 212013, China.

Received: 19 December 2021 Accepted: 13 May 2022
Published online: 23 June 2022

References

1. Chiuta S, et al. (2013) "Reactor technology options for distributed hydrogen generation via ammonia decomposition: A review," International Journal of Hydrogen Energy, pp. 14968–14991. https://doi.org/10.1016/j.ijhydene.2013.09.067.
2. Zamfirescu C, Dincer I (2009) Ammonia as a green fuel and hydrogen source for vehicular applications. Fuel Process Technol 90(5):729–737. https://doi.org/10.1016/j.fuproc.2009.02.004
3. Dimitriou P, Javaid R (2020) A review of ammonia as a compression ignition engine fuel. International Journal of Hydrogen Energy. Elsevier Ltd, pp. 7098–7118. https://doi.org/10.1016/j.ijhydene.2019.12.209.
4. Kobayashi H et al (2019) Science and technology of ammonia combustion. Proc Combust Inst 37(1):109–133. https://doi.org/10.1016/j.proci.2018.09.029
5. Valera-Medina A et al (2018) "Ammonia for power," Progress in Energy and Combustion Science. Elsevier Ltd, pp. 63–102. https://doi.org/10.1016/j.pecs.2018.07.001.
6. Mørch CS et al (2011) Ammonia/hydrogen mixtures in an SI-engine: Engine performance and analysis of a proposed fuel system. Fuel 90(2):854–864. https://doi.org/10.1016/j.fuel.2010.09.042
7. Reiter AJ, Kong SC (2011) Combustion and emissions characteristics of compression-ignition engine using dual ammonia-diesel fuel. Fuel 90(1):87–97. https://doi.org/10.1016/j.fuel.2010.07.055
8. Chai, W.S. et al. (2021) "A review on ammonia, ammonia-hydrogen and ammonia-methane fuels," Renewable and Sustainable Energy Reviews. Elsevier Ltd. https://doi.org/10.1016/j.rser.2021.111254.
9. Crutzen PJ, Brauch HG (2016) Springer briefs on pioneers in science and practice nobel laureates A Pioneer on Atmospheric Chemistry and Climate Change in the Anthropocene. Available at: http://www.afes-press-books.de/html/SpringerBriefs_PSP.htm.
10. de Diego LF et al (1996) Influence of operating parameters on NOx and N20 axial profiles in a circulating fluidized bed combustor, Fuel.
11. Hill SC, Smoot LD (2000) Modeling of nitrogen oxides formation and destruction in combustion systems. Available at: www.elsevier.com/locate/pecs.
12. Johnsson JE (1993) Formation and reduction of nitrogen oxides in fluidized-bed combustion.
13. Miller JA, Bowman CT (1989) Mechanism and modeling of nitrogen chemistry in combustion. Prog Energy Combust Sci 15(4):287–338. https://doi.org/10.1016/0360-1285(89)90017-8
14. Bowman CT (1992) Invited lecture control of combustion-generated nitrogen oxide emissions: Technology driven by regulation.
15. Glarborg P, Jensen AD, Johnsson JE (2003) Fuel nitrogen conversion in solid fuel fired systems. Progress in Energy and Combustion Science. Elsevier Ltd, pp. 89–113. https://doi.org/10.1016/S0360-1285(02)00031-X.
16. Glarborg, P. (2007) "Hidden interactions-Trace species governing combustion and emissions," Proceedings of the Combustion Institute, 31 I(1), pp. 77–98. https://doi.org/10.1016/j.proci.2006.08.119.
17. Mathieu O, Petersen EL (2015) Experimental and modeling study on the high-temperature oxidation of Ammonia and related NOx chemistry. Combust Flame 162(3):554–570. https://doi.org/10.1016/j.combustflame.2014.08.022
18. Mei B et al (2019) Experimental and kinetic modeling investigation on the laminar flame propagation of ammonia under oxygen enrichment and elevated pressure conditions. Combust Flame 210:236–246. https://doi.org/10.1016/j.combustflame.2019.08.033
19. Song Y et al (2016) Ammonia oxidation at high pressure and intermediate temperatures. Fuel 181:358–365. https://doi.org/10.1016/j.fuel.2016.04.100
20. Shrestha KP et al (2018) Detailed Kinetic Mechanism for the Oxidation of Ammonia Including the Formation and Reduction of Nitrogen Oxides. Energy Fuels 32(10):10202–10217. https://doi.org/10.1021/acs.energyfuels.8b01056
21. Hayakawa A et al (2015) Laminar burning velocity and Markstein length of ammonia/air premixed flames at various pressures. Fuel 159:98–106. https://doi.org/10.1016/j.fuel.2015.06.070
22. Glarborg, P. et al. (2018) "Modeling nitrogen chemistry in combustion," Progress in Energy and Combustion Science. Elsevier Ltd, pp. 31–68. https://doi.org/10.1016/j.pecs.2018.01.002.
23. R Li et al 2019 Chemical mechanism development and reduction for combustion of NH3/H2/CH4 mixtures Fuel 257 https://doi.org/10.1016/j.fuel.2019.116059
24. Klippenstein SJ et al (2018) Theory and modeling of relevance to prompt-NO formation at high pressure. Combust Flame 195:3–17. https://doi.org/10.1016/j.combustflame.2018.04.029
25. Hayakawa A et al (2021) Experimental and numerical study of product gas characteristics of ammonia/air premixed laminar flames stabilized in a stagnation flow. Proc Combust Inst 38(2):2409–2417. https://doi.org/10.1016/j.proci.2020.07.030
26. Gaydon AG (1974) The Spectroscopy of Flames. Springer, Netherlands, Dordrecht. https://doi.org/10.1007/978-94-009-5720-6
27. Schott GL, Blair LS, Morgan JD (1973) Physical Chemistry Exploratory Shock-Wave Study of Thermal Nitrogen Trifluoride Decomposition and Reactions of Nitrogen Trifluoride and Dinitrogen Tetrafluoride with Hydrogen1ab. Available at: https://pubs.acs.org/sharingguidelines.
28. Roose TR, Hanson RK, Kruger CH (1981) A shock tube study of the decomposition of no in the presence of NH 3.
29. Yi Y et al (2017) Plasma-Triggered CH4/NH3 Coupling Reaction for Direct Synthesis of Liquid Nitrogen-Containing Organic Chemicals. ACS Omega 2(12):9199–9210. https://doi.org/10.1021/acsomega.7b01060
30. Ohashi, K. et al. (1989) Alignment Dependence of the NH, Chemiluminescence in the Reaction of Ar('P) Atoms with the Aligned NH, Molecules, J. Phys. Chem.
31. Mashruk S (2020) Nitric oxide formation analysis using chemical reactor modelling and laser induced fluorescence measurements on industrial swirl flames.
32. Shaddix CR (2017) A new method to compute the proper radiant heat transfer correction of bare-wire thermocouple measurements.
33. Kee RJ, Rupley FM, Miller J.A. (1989) Chemkin-II: A fortran chemical kinetics package for the analysis of gas-phase chemical kinetics.
34. Mashruk S, Xiao H, Valera-Medina A (2021) Rich-Quench-Lean model comparison for the clean use of humidified ammonia/hydrogen combustion systems. Int J Hydrogen Energy 46(5):4472–4484. https://doi.org/10.1016/j.ijhydene.2020.10.204
35. Mashruk S et al. (2021) Numerical Analysis on the Evolution of NH2 in Ammonia/hydrogen Swirling Flames and Detailed Sensitivity Analysis under Elevated Conditions,. Combustion Science and Technology [Preprint]. https://doi.org/10.1080/00102202.2021.1990897.
36. M Guteša Božo et al (2021) Humidified ammonia/hydrogen RQL combustion in a trigeneration gas turbine cycle Energy Convers Manage 227 https://doi.org/10.1016/j.enconman.2020.113625
37. Vigueras-Zuniga MO et al. (2020) Numerical predictions of a swirl combustor using complex chemistry fueled with ammonia/hydrogen blends. Energies, 13(2). https://doi.org/10.3390/en13020288.
38. Valera-Medina A, Syred N, Bowen P (2013) Central recirculation zone visualization in confined swirl combustors for terrestrial energy. J Propul Power 29(1):195–204. https://doi.org/10.2514/1.B34600
39. A Bertolino et al (2021) An evolutionary, data-driven approach for mechanism optimization: theory and application to ammonia combustion Combust Flame 229 https://doi.org/10.1016/j.combustflame.2021.02.012
40. Mei B et al (2021) Characterizing ammonia and nitric oxide interaction with outwardly propagating spherical flame method. Proc Combust Inst 38(2):2477–2485. https://doi.org/10.1016/j.proci.2020.07.133
41. Han X, Lavadera L, Konnov AA (2021) An experimental and kinetic modeling study on the laminar burning velocity of NH3+N2O+air flames. Combust Flame 228:13–28. https://doi.org/10.1016/j.combustflame.2021.01.027
42. X Zhang et al 2021 Combustion chemistry of ammonia/hydrogen mixtures: Jet-stirred reactor measurements and comprehensive kinetic modeling Combust Flame 234https://doi.org/10.1016/j.combustflame.2021.111653
43. Stagni A et al (2020) An experimental, theoretical and kinetic-modeling study of the gas-phase oxidation of ammonia. Reaction Chemistry and Engineering 5(4):696–711. https://doi.org/10.1039/c9re00429g

44. Han X et al (2019) Experimental and kinetic modeling study of laminar burning velocities of NH3/air, NH3/H2/air, NH3/CO/air and NH3/CH4/air premixed flames. Combust Flame 206:214–226. https://doi.org/10.1016/J.COMBUSTFLAME.2019.05.003
45. S Persis de et al. (2020) NO formation in high pressure premixed flames: Experimental results and validation of a new revised reaction mechanism Fuel 260 https://doi.org/10.1016/j.fuel.2019.116331
46. Han X et al (2021) Experimental and kinetic modeling study of NO formation in premixed CH4+O2+N2 flames. Combust Flame 223:349–360. https://doi.org/10.1016/j.combustflame.2020.10.010
47. Capriolo G et al (2021) An experimental and kinetic modeling study on nitric oxide formation in premixed C3 alcohols flames. Proc Combust Inst 38(1):805–812. https://doi.org/10.1016/J.PROCI.2020.07.051
48. Burcat A, Ruscic B (2005) Third Millennium Ideal Gas and Condensed Phase Thermochemical Database for Combustion with Updates from Active Thermochemical Tables. Available at: www.anl.gov.
49. Li Y, Sarathy SM (2020) Probing hydrogen–nitrogen chemistry: A theoretical study of important reactions in NxHy, HCN and HNCO oxidation. Int J Hydrogen Energy 45(43):23624–23637. https://doi.org/10.1016/J.IJHYDENE.2020.06.083
50. Davidson DF et al (1990) A Pyrolysis Mechanism for Ammonia.
51. Glarborg P et al (2021) On the rate constant for NH2+HO2and third-body collision efficiencies for NH2+H(+M) and NH2+NH2(+M). J Phys Chem A 125(7):1505–1516. https://doi.org/10.1021/acs.jpca.0c11011
52. Diévart P, Catoire L (2020) Contributions of Experimental Data Obtained in Concentrated Mixtures to Kinetic Studies: Application to Monomethylhydrazine Pyrolysis. J Phys Chem A 124(30):6214–6236. https://doi.org/10.1021/acs.jpca.0c03144
53. Kanno N, Kito T (2020) Theoretical study on the hydrogen abstraction reactions from hydrazine derivatives by H atom. Int J Chem Kinet 52(8):548–555. https://doi.org/10.1002/kin.21370
54. Nguyen TL, Stanton JF (2019) Ab initio thermal rate coefficients for H + NH 3 ⇌ H 2 + NH 2. Int J Chem Kinet 51(5):321–328. https://doi.org/10.1002/kin.21255
55. Chavarrio Cañas JE et al (2022) Probing the gas-phase oxidation of ammonia: Addressing uncertainties with theoretical calculations Combust Flame 235 https://doi.org/10.1016/j.combustflame.2021.111708
56. Chen X, Fuller ME, Goldsmith F (2018) Reaction Chemistry & Engineering Decomposition Kinetics for HONO and HNO 2. 1. Available at: http://rsc.li/reaction-engineering.
57. Klippenstein SJ et al (2009) Thermal decomposition of NH2OH and subsequent reactions: Ab initiotransition state theory and reflected shock tube experiments. J Phys Chem A 113(38):10241–10259. https://doi.org/10.1021/jp905454k
58. Varga T et al (2016) Development of a Joint Hydrogen and Syngas Combustion Mechanism Based on an Optimization Approach. Int J Chem Kinet 48(8):407–422. https://doi.org/10.1002/kin.21006
59. Lamoureux N et al (2016) Modeling of NO formation in low pressure premixed flames. Combust Flame 163:557–575. https://doi.org/10.1016/j.combustflame.2015.11.007
60. Cemal Benim, A. and Syed, K.J. (2015) Flashback mechanisms in lean premixed gas turbine combustion.